

Drosophila Amphiphysin is a Post-Synaptic Protein Required for Normal Locomotion but Not Endocytosis

Peter A. Leventis^{1,3,*}, Brenda M. Chow^{2,3,*},
Bryan A. Stewart^{3,5}, Balaji Iyengar⁴,
Ana Regina Campos⁴
and Gabrielle L. Boulianne^{1,2,3,**}

Departments of ¹Zoology and ²Molecular and Medical Genetics, University of Toronto, Toronto, Canada

³Program in Developmental Biology, The Hospital for Sick Children, 555 University Avenue, Toronto, Ontario, Canada, M5G 1X8,

⁴Department of Biology, McMaster University, Hamilton, Ontario, Canada, L8S 4K1

⁵Current address: Division of Life Sciences, University of Toronto at Scarborough, 1265 Military Trail, Toronto, Ontario, Canada, M1C 1A4

**Corresponding author: Dr Gabrielle L. Boulianne, gboul@sickkids.ca

Clathrin-mediated endocytosis is required to recycle synaptic vesicles for fast and efficient neurotransmission. Amphiphysins are thought to be multiprotein adaptors that may contribute to this process by bringing together many of the proteins required for endocytosis. Their *in vivo* function, however, has yet to be determined. Here, we show that the *Drosophila* genome encodes a single *amphiphysin* gene that is broadly expressed during development. We also show that, unlike its vertebrate counterparts, *Drosophila* Amphiphysin is enriched postsynaptically at the larval neuromuscular junction. To determine the role of *Drosophila* Amphiphysin, we also generated null mutants which are viable but give rise to larvae and adults with pronounced locomotory defects. Surprisingly, the locomotory defects cannot be accounted for by alterations in the morphology or physiology of the neuromuscular junction. Moreover, using stimulus protocols designed to test endocytosis under moderate and extreme vesicle cycling, we could not detect any defect in the neuromuscular junction of the *amphiphysin* mutant. Taken together, our findings suggest that Amphiphysin is not required for viability, nor is it absolutely required for clathrin-mediated endocytosis. However, *Drosophila* Amphiphysin function is required in both larvae and adults for normal locomotion.

Key words: actin, amphiphysin, endocytosis, synaptic vesicle recycling

Received 6 August 2001, revised and accepted for publication 27 August 2001

Clathrin-mediated endocytosis has been widely implicated as a mechanism to regenerate and maintain pools of synaptic vesicles (SVs) during neurotransmission. It is thought to be initiated by the formation of clathrin-coated pits through a process involving clathrin and its adaptor proteins, AP180 and AP2 (1). 'Pinching off' of the vesicle is thought to require the function of the GTPase dynamin (2). Dynamin has been suggested to act as a 'popase' by wrapping around the neck of a budding vesicle and 'popping' the vesicle off the end of the neck (3), or as a regulator to ensure that a neck is the correct diameter (4).

Other cytosolic proteins are also believed to play a role in clathrin-mediated endocytosis. These include the inositol-5'-phosphatase, synaptojanin (5), the lysophosphatidic acid acyl transferase endophilin (6) and amphiphysin (7–10). In vertebrates, two amphiphysin homologs, amphiphysin 1 and 2, have been found to be highly concentrated in nerve terminals (7–9) and are composed of three domains. The amino terminal BAR domain (9) named after the original family members (Bin1/Amphiphysin 1/Rvs167), is predicted to form coiled-coil structures that are involved in dimerization and interaction with lipid membranes (11). Bin1 is an alternatively spliced product of the amphiphysin 2 gene in mammals, whereas Rvs167 is found in budding yeast. The central region binds, through distinct sites, to clathrin (8,12–14), endophilin (14), and the α -adaptin subunit of AP2 (10,15). Finally, the carboxy terminus contains an SH3 domain that binds both dynamin (16–18) and synaptojanin (19). The ability of amphiphysin to bind to several components of the endocytic machinery strongly suggests that amphiphysin may function as a multiprotein adaptor to assemble a number of proteins required for SV endocytosis.

To date, the function of amphiphysin has largely been studied using dominant-negative constructs or by injecting peptides into neuronal or non-neuronal cells. These studies have shown that overexpression of the clathrin/AP2 binding domain of amphiphysin can block transferrin receptor endocytosis in HeLa cells, presumably by blocking the interaction of amphiphysin with clathrin and AP2 (20). Similarly, overexpression of the SH3 domain that binds both dynamin and synaptojanin has been shown to block endocytosis in several different cell lines (10,17). Presynaptic injection of a GST-fusion protein consisting of the SH3 domain of human amphiphysin 1 into the lamprey giant reticulospinal synapse also results in the accumulation of coated pits and a large decrease in amplitude of excitatory postsynaptic potentials during prolonged stimulation, consistent with disruption of clathrin-mediated SV endocytosis (17). Interestingly, loss-of-

*These authors contributed equally to the work described in this article.

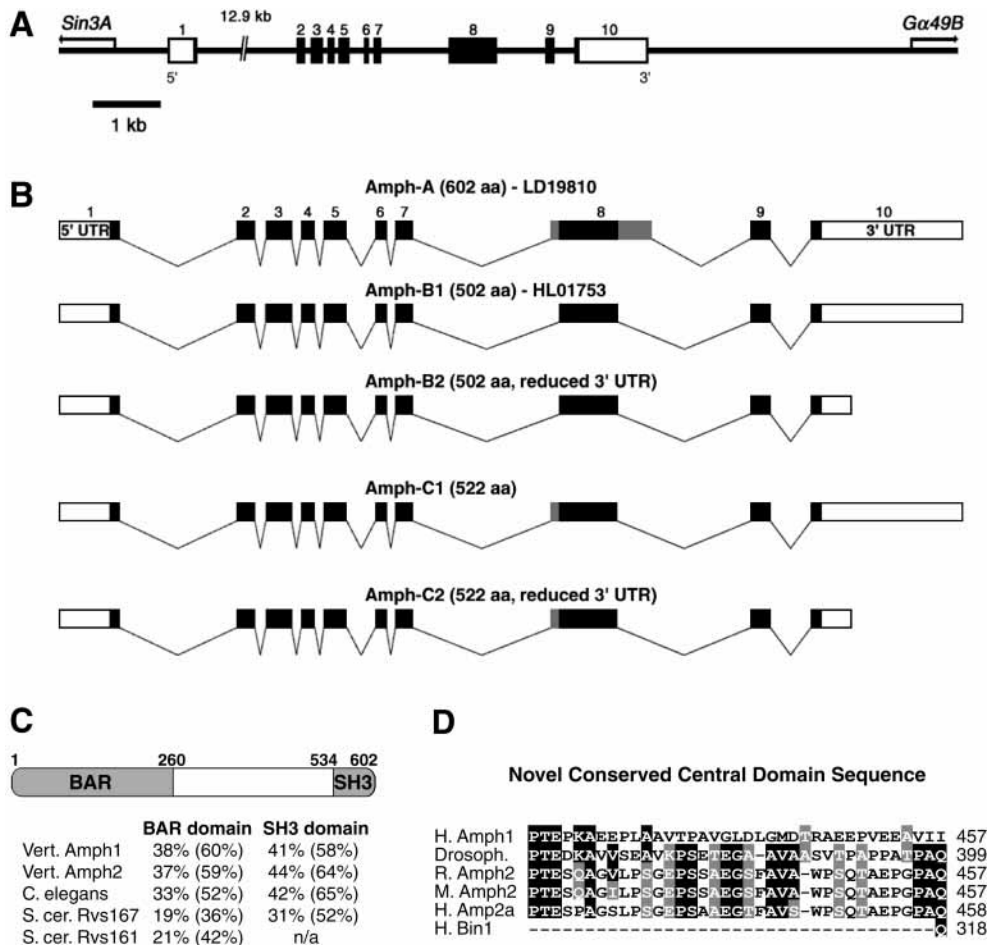


Figure 1: (A) *amph* consists of 10 exons (boxes) over 18425 bp, with a large intron of 12.9 kb separating the first two exons. Exons 1 and 10 contain both untranslated sequence (open boxes) and parts of the ORF (filled boxes). The two genes flanking *amph*, *Sin3A* and *Ga49B*, are shown with their orientation. (B) The structure of the various *amph* cDNAs identified is shown. Amph-A represents the longest clone identified in our screens. The additional isoforms differ primarily within exon 8 which encodes part of the central domain and the 3' UTR. Variably spliced parts of exons are shaded grey to highlight these regions. (C) The predicted three-domain structure of amphiphysin is shown. Below is indicated the percent identity and similarity (bracket) between amphiphysins from different species within the BAR and SH3 domain. (D) An additional domain was identified within the central portion of amphiphysin that is highly conserved between *Drosophila* Amph and vertebrate amphiphysin 2 isoforms. Amino acid identities are shaded in black, whereas conserved residues are shaded in grey. H = human; M = mouse; R = rat.

function mutations in the yeast orthologs of amphiphysin, RVS167p and a related protein RVS161p, not only exhibit defects in endocytosis (21,22) but also show reduced viability upon nutrient starvation (23,24), budding defects (24) and delocalized actin patches (22,24–26). This actin phenotype appears to be due to the inability of the yeast cdk5 homolog, Pho85, to signal via Rvs161p/Rvs167p to the cortical actin cytoskeleton. More recently, vertebrate amphiphysins have also been shown to play a role in cortical actin dynamics and to interact with cdk5 (27). Taken together, these data suggest that in addition to a role in SV endocytosis, amphiphysin may have additional cell biological roles. Therefore, to gain further insight into the *in vivo* roles of amphiphysin, we generated and characterized null mutations in the *Drosophila* amphiphysin gene (*amph*).

Results

Molecular organization of the *Drosophila* amphiphysin gene

As a first step to identify the *in vivo* function of amphiphysin, we characterized the *amphiphysin* (*amph*) gene from *Drosophila*. Unlike vertebrates, the *Drosophila* genome contains a single *amph* gene (28,29) that gives rise to multiple isoforms by alternative splicing. The entire gene is contained within 18.5 kb of genomic DNA and is flanked at the 5' end by the *Sin3A* gene which encodes a transcription corepressor (30,31) and at the 3' end by the *Ga49B* gene which encodes an eye-specific subunit of a heterotrimeric G-protein GTPase (32,33). The predicted intron/exon structure of *Drosophila* *amph* is illustrated in Figure 1(A).

Consistent with a previous report (28) we found that *amph* gives rise to a 3162 bp transcript. In addition, we have also identified four other predicted isoforms of *amph* (2922 bp, 2862 bp, 2117 bp, and 2057 bp) by sequencing another EST (HL01753) and several positive clones isolated from a cDNA library screen (Figure 1B). All isoforms identified arise from alternative splicing within exon 8. Additionally, the two shortest isoforms also contain a shorter 3' UTR due to polyadenylation at a cryptic site 120 bp after the stop codon. The longest isoform encodes a predicted 602 amino acid product, whereas the shorter isoforms predict proteins of 522 and 502 aa, respectively.

Overall, the predicted full-length protein is approximately 30% identical to rat amphiphysins 1 and 2, and 24% identical to the predicted *C. elegans* amphiphysin. The highest degree of similarity is in the N-terminal BAR domain which shares ~38% identity and ~60% similarity with vertebrate amphiphysin 1 and 2 (Figure 1C). This domain is predicted to form coiled-coil structures that are involved in dimerization and interaction with lipid membranes and is encoded by exons 1–6 (11). Similarly, the C-terminal SH3 domain, which binds both dynamin and synaptojanin (34), is also highly conserved and is encoded by exons 9 and 10 (Figure 1C). In contrast, the central domain which binds clathrin, endophilin, and the α -adaptin subunit of AP2 is poorly conserved and the consensus sequences for binding these proteins are absent. However, within this central domain, we have identified another region that is conserved between *Drosophila* Amph and vertebrate amphiphysin 2 (but not Bin-1 splice variants). This region lies between amino acids 363 and 398 of *Drosophila* Amph and is encoded by the nonvariably spliced part of exon 8. This domain starts 2 amino acid residues after the second clathrin binding domain in some forms of amphiphysin 2 and is partially conserved in amphiphysin 1 (Figure 1D).

Amph is broadly expressed during development

To examine the temporal and spatial distribution of Amph during development, we generated rabbit polyclonal antibodies to a full-length (602 aa) His₆-tagged Amph protein. We found on Western blots that this antiserum recognized a single band corresponding to the recombinant Amph protein, while none were detected using the pre-immune serum, even after prolonged exposures (data not shown). We then performed Western blots on lysates from *Drosophila* at different stages of development. At all developmental stages examined, we observed an 85-kDa band, a cluster of bands at 80 kDa that may represent additional splice variants or different phospho-isoforms of Amph and a 45-kDa band that may be the product of an as-of-yet unidentified transcript, or a proteolytic degradation product (Figure 2A). However, all of the isoforms appear to be down-regulated in both first larval instars and pupae. Moreover, all 3 major isoforms are absent in null mutants (discussed below) and are not detected by the pre-immune serum. As with vertebrate amphiphysin (7), *Drosophila* Amph has a reduced mobility on SDS-PAGE gels compared to the predicted size of the protein (~85 kDa vs. 65.9 kDa predicted). We also examined the distribution of Amph in several tissues including body wall/muscle, central nervous system (CNS) and imaginal discs (Figure 2B). We found that all of the isoforms could be detected in whole larvae and in the body wall, which is comprised primarily of muscle. In contrast, the 45 kDa isoform appears to be absent or strongly down-regulated in both the CNS and imaginal discs (Figure 2B). Multiple isoforms of amphiphysin have also been observed in vertebrates, including brain-specific and ubiquitous forms. This suggests that in addition to a role in synaptic vesicle-mediated endocytosis, amphiphysins may also have additional cell biological functions within specific tissues.

to further investigate the distribution of Amph, we also per-

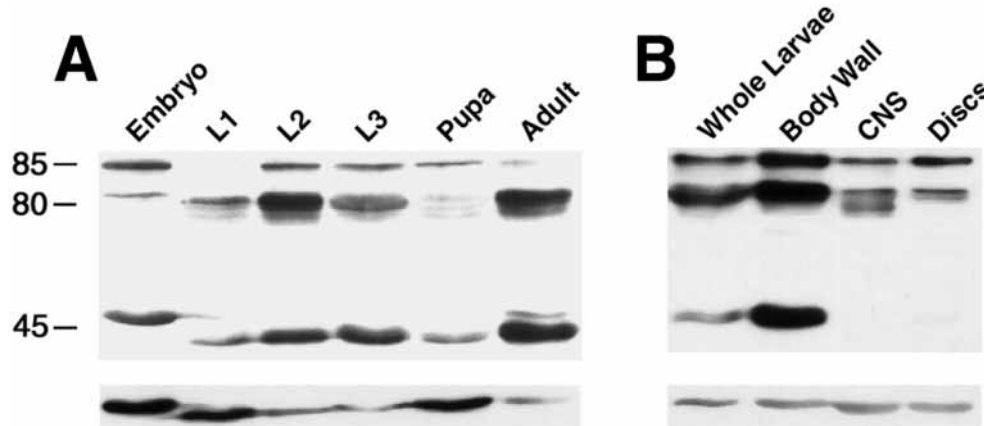


Figure 2: Expression of Amph was examined using a rabbit polyclonal antibody raised against a full-length fusion protein. (A) Western blot analysis of 20 μ g total protein lysates made from different developmental stages (embryos, first, second and third instar larvae, early pupae, and adults) of a wildtype line (Oregon-R) separated by SDS-PAGE. Anti-Amph 9184 antiserum (1 : 1500) detects at least three different bands at 45, 80, and 85 kDa at all stages. (B) Western blot analysis of 20 μ g total protein lysates made from wildtype whole larvae, dissected CNS, imaginal discs, and body wall of wandering third instar larvae separated by SDS-PAGE. Three major immunoreactive bands are seen in whole third instar larvae and in the body wall, which contains mostly muscle. Two are seen in the CNS and the imaginal discs. The bottom panel shows anti- β -tubulin which was used as a loading control.

formed immunohistochemical and immunofluorescence staining of embryos and third instar larval CNS and imaginal discs. We found that Amph was widely expressed in embryos and larvae (Figure 3). Specifically, we found that Amph is first detected in embryos at the onset of cellularization at the sites of developing membranes (Figure 3A,B). At later stages, we observed staining in epithelial tissues, the foregut and hindgut (Figure 3C,D). In contrast, we did not observe any Amph expression in either the embryonic

nervous system or muscle. In third larval instars, Amph can be detected at high levels in both larval epithelial cells (Figure 3E) and muscles (Figure 3F), with intense staining at the neuromuscular junction (Figure 3F, arrow). In addition, and consistent with our Western blot analysis, we also observed ubiquitous expression of Amph in both imaginal discs and the CNS (data not shown). No staining was observed in either embryos or larvae from null mutants (described below).

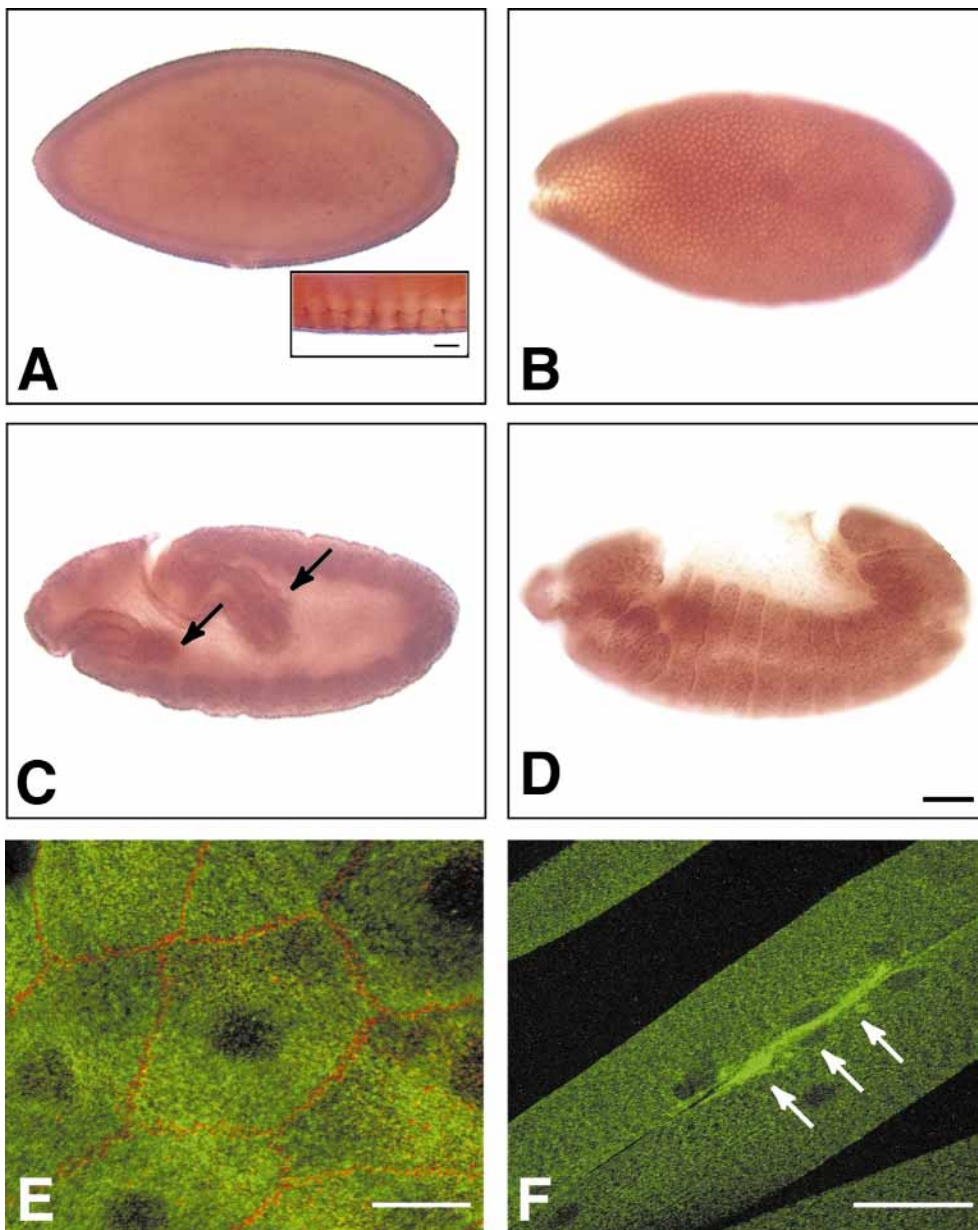


Figure 3: Amph localization in embryos and third larval instar. Amph is broadly distributed throughout early embryos. In cellular blastoderm embryos (A,B), it is localized to epithelial cells and appears to be concentrated at cellular membranes (A, inset and B). During later stages of embryogenesis, Amph is localized in the gut (C, arrows) and abdominal segments (D). Immunofluorescent staining of Amph in third larval instars demonstrates punctate cytoplasmic staining in epithelial cells (E) and muscle (F), with intense staining at the neuromuscular junction (F, arrows). Both images are from stacked confocal slices. Epithelial cells in E have also been stained with anti-crumb (in red) to outline the plasma membrane. Scale bars are 50 μm in A–D (with inset in A, 8 μm), 20 μm in E and 50 μm in F.

Amphiphysin is localized postsynaptically at the larval neuromuscular junction

Since amphiphysin has been widely implicated in synaptic vesicle endocytosis, we also examined the subcellular distribution of Amph at the larval neuromuscular junction (NMJ). Vertebrate amphiphysins have previously been shown to be highly enriched at nerve terminals and associated with SVs. To determine if *Drosophila* Amph was similarly found at sites of SV endocytosis, we used immunofluorescence techniques and confocal microscopy. We found that *Drosophila* Amph was highly expressed at the NMJ (Figure 4). To determine if synaptic Amph was localized pre- or postsynaptically, we performed co-immunolocalization studies with the presynaptic protein, cysteine string protein (CSP), and with UAS-CD8::Sh-GFP that is driven postsynaptically by MHC-GAL4. As expected, we found that CSP and CD8::Sh-GFP had discrete, nonoverlapping distributions (Figure 4A). Surprisingly, double labeling of wildtype NMJs demonstrated that CSP and Amph did not colocalize (Figure 4B). However, Amph

and CD8::Sh-GFP showed a high degree of colocalization at the NMJ, although Amph was more diffusely localized (Figure 4C). Therefore, within the limits of our detection ability, Amph is not localized presynaptically, but is present at the synaptic surface of the muscle cell.

Generation and characterization of amph mutants

The broad tissue distribution and postsynaptic localization of Amph was unexpected, based on prior results obtained in vertebrates. To further characterize the function of Amph, we therefore created a series of *amph* mutants by imprecise excision of a transposable P-element, *EP(2)2175*, inserted 39bp 5' to the *amph* transcription start site (Figure 5A; Berkeley Drosophila Genome Project (BDGP), unpublished). In total, we generated four independent deletions which removed various portions of the *amph* gene and failed to complement each other (Figure 5A). All of the *amph* mutants are homozygous viable, although the larvae and adults appeared sluggish (see below). Using a combination of Southern blot

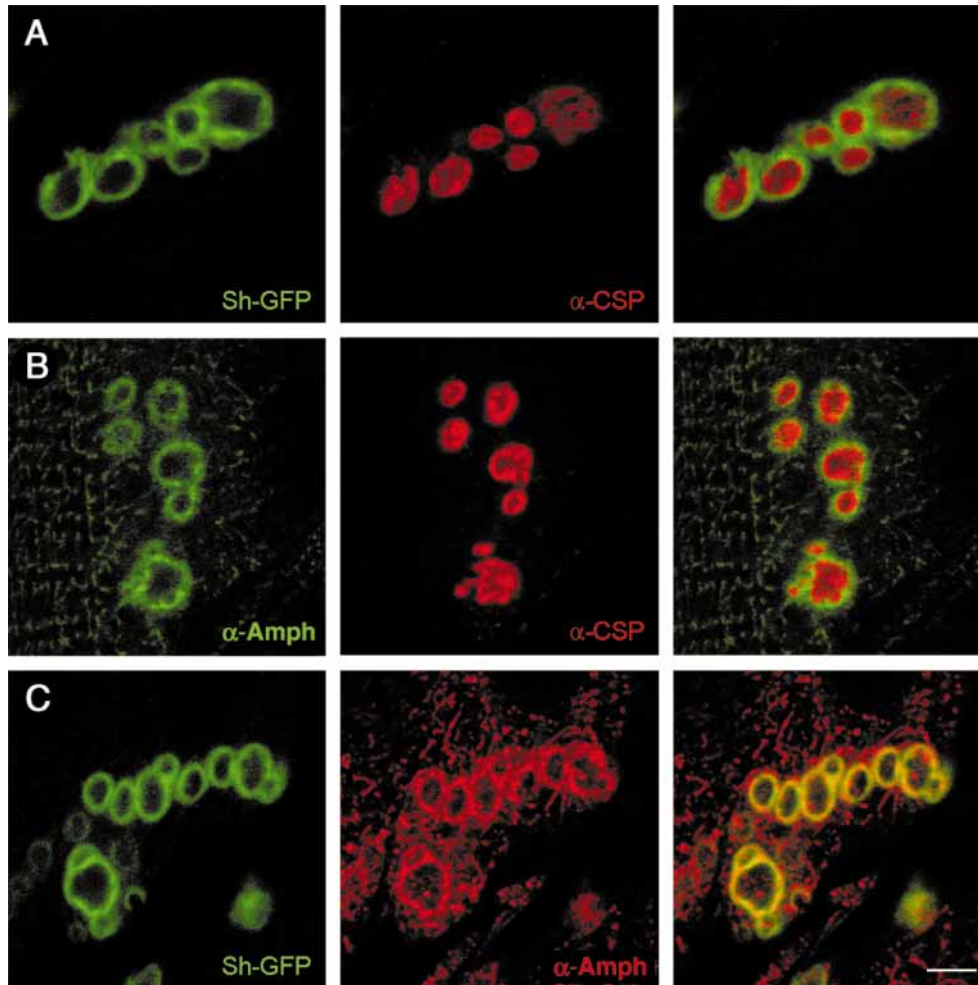


Figure 4: Amph localizes to the post-, but not presynaptic membrane at the NMJ. (A) The presynaptic marker cysteine string protein (CSP; red) and the postsynaptic marker CD8::Sh-GFP (green) do not colocalize at the NMJ. (B) Amph (green) and CSP (red) also do not colocalize. (C) Amph (red) and CD8::Sh-GFP (green) do colocalize at the NMJ, showing that Amph is found not at the presynaptic membrane, but at the postsynaptic membrane. Scale bar = 2.5 μ m.

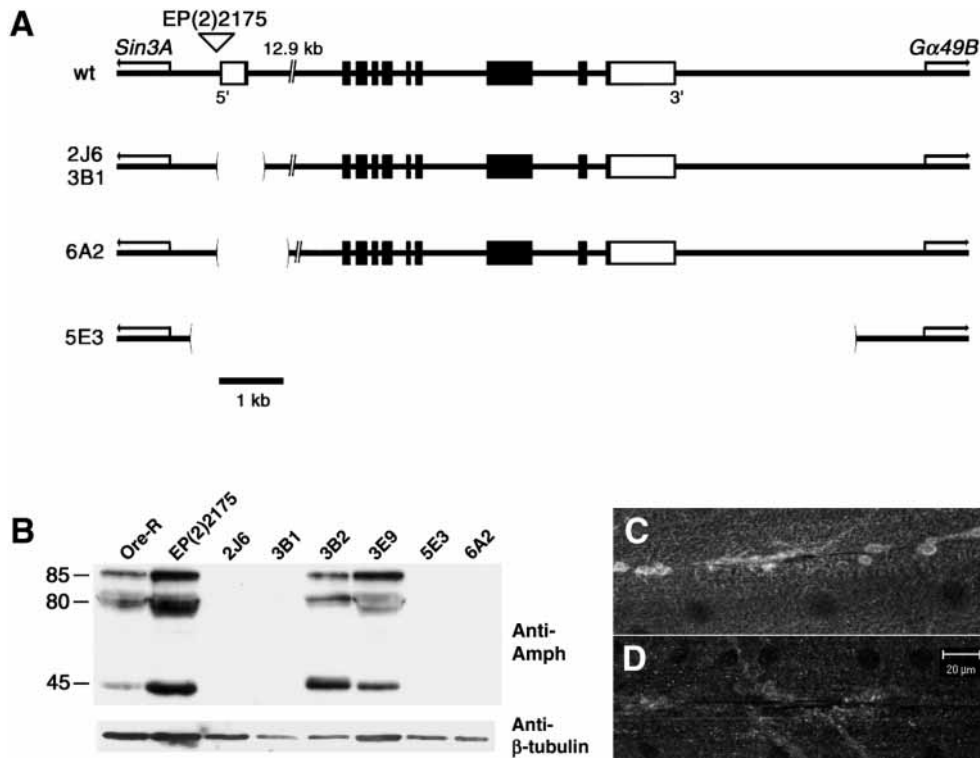


Figure 5: *amph* mutants are protein null. (A) *amph* mutants were generated by imprecise excision of the EP line EP(2)2175. The breakpoints of the four deletions analyzed are illustrated. The excision mutants *amph*^{2J6} and *amph*^{3B1} (733bp deletion), and *amph*^{6A2} (1109bp deletion) are missing exon 1 along with parts of the first intron. *amph*^{5E3} is an excision of the entire gene (~20kb), but neither *Sin3A* nor *Gα49B* is disrupted. Scale bar = 1 kb (B) Anti-Amph recognizes three bands in wildtype (Ore-R), original P-element line (EP2175), and precise excision lines (*amph*^{3B2} and *amph*^{3E9}), but does not recognize any bands in the excision lines *amph*^{2J6}, *amph*^{3B1}, *amph*^{5E3}, and *amph*^{6A2}. In all experiments, anti-β-tubulin was used to demonstrate equal loading. (C) Amph protein can be detected at the NMJ of wildtype larvae but is absent from mutants (D).

and PCR analyses, we found that three lines had deletions of the first exon (*amph*^{2J6}, *amph*^{3B1}, *amph*^{6A2}), whereas *amph*^{5E3} represented a deletion of the entire gene. Importantly, none of the deletions disrupted either of the flanking genes, *Sin3A* and *Gα49B*, indicating that these mutations only affect *amph* (data not shown).

To determine if any of the mutants produced Amph protein, we performed Western blot analysis on lysates from control and mutant third instar larvae. Not surprisingly, the genetic null mutant *amph*^{5E3} was also protein null (Figure 5B). Additionally, we found that the removal of exon 1 also led to a complete elimination of Amph protein expression. In contrast, Amph protein was detected from lysates generated from wildtype flies, the original EP insertion line and two precise excision lines (*amph*^{3B2}, *amph*^{3E9}). Consistent with these results, we also found that Amph was present at the NMJ of wildtype larvae and controls but not in mutants (Figure 5C).

***amph* mutants exhibit locomotion defects**

As mentioned above, all of the *amph* mutants identified were viable but gave rise to larvae and adults that appeared slug-

gish and slower in their movements. For example, while adult flies are capable of hopping they are essentially flightless. To further quantify any potential locomotory defects, we measured the total distance traveled by third instar larvae over 30s (35). The genetic null *amph*^{5E3} mutant larvae showed about a 70% reduction in movement (Figure 6). They moved (mean ± standard error of the mean) 51.1 ± 12.76 pixels (n = 17), compared with 167.4 ± 9.83 pixels (n = 16) for the precise excision line *amph*^{3E9}, and 161.1 ± 11.64 pixels (n = 16) for the original P-element line EP(2)2175 (Figure 6A,B). This difference was significant in both cases (p < 0.0001).

***amph* mutants exhibit no defects in synaptic morphology, physiology or vesicle recycling**

Locomotory defects such as we have observed in our *amph* mutants could reflect defects in synaptic morphology or physiology. To determine if *amph* mutants exhibited any alterations in NMJ morphology, we compared anti-horse-radish peroxidase (HRP)-FITC stained NMJs (36) from mutant and control third instar larvae and found no difference in either the number of boutons or the amount of branching (data not shown). Therefore, we concluded that Amph is not required for the normal morphogenesis of the NMJ. Since no

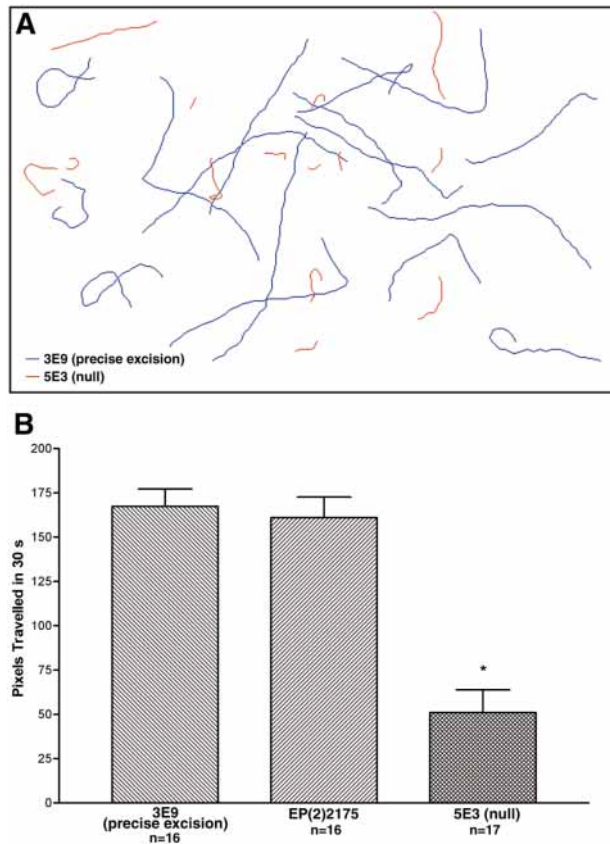


Figure 6: *amph* mutant larvae have defects in locomotion. A The distance traveled by 90-h-old third instar larvae was recorded in the dark over 30 s. Sample traces of 16 control larvae (blue) and 17 mutant larvae (red). (B) *amph*^{5E3} larvae moved only 51.1 ± 12.76 pixels ($n = 17$; mean \pm standard error of the mean), compared with 167.4 ± 9.83 pixels ($n = 16$) for the precise excision line *amph*^{3E9}, and 161.1 ± 11.64 pixels ($n = 16$) for the original P-element line *EP(2)2175*. This difference was significant ($p < 0.0001$).

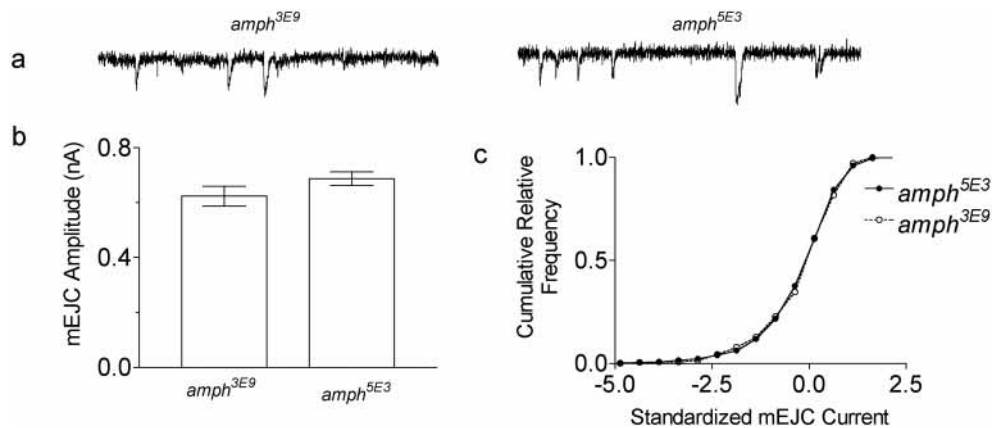


Figure 7: Miniature excitatory junctional currents measured from *amph* mutants. (A) Examples of mEJCs recorded from the mean mEJC amplitude measured from *amph*^{3E9} and mutant *amph*^{5E3} muscles. (B) Summary of mEJC amplitude data collected from *amph*^{3E9} ($n = 7$ cells, 395 mEJCs) and *amph*^{5E3} ($n = 6$ cells, 305 mEJCs). (C) The shape of the cumulative relative frequency distribution of standardized mEJC amplitudes was not different between the two genotypes. The data were standardized as described in Frerking et al. (46).

phenotypic difference was detected in any of the mutants and they were all protein null, all subsequent experiments were performed with a single *amph* mutant line, *amph*^{5E3} (Figure 7).

To determine whether the locomotory defects in *amph* mutants were due to impaired synaptic physiology, we then characterized synaptic currents from neuromuscular junctions of third instar larvae. Because Amph is predominantly localized postsynaptically, we first analyzed spontaneously occurring quantal events from both the precise excision line and the mutant *amph*^{5E3} to determine if there were any effects on glutamate receptors (Figure 7). We found the amplitude of mEJCs (excitatory junctional current) from *amph*^{5E3} was 0.68 ± 0.02 nA (305 mEJCs from 6 cells), while in *amph*^{3E9} mEJCs were 0.62 ± 0.03 nA (395 mEJCs from 7 cells). We first conducted a single classification ANOVA on the individual cells within each genotype to determine if we could pool these raw data, but we found that there was significant variation ($p < 0.01$) within each genotype. Therefore, rather than pooling the data, we carried out a nested ANOVA on the mEJC amplitudes, as described in Sokal and Rohlf (37). This procedure enabled us to take into account the variation between cells within each genotype while testing for differences between the mutants and controls. When analyzed this way, we found that while there were significant differences ($p < 0.01$) within the genotypes, there was no significant difference in mEJC amplitude between the mutant and controls. Thus we conclude that the *amph* mutant does not alter the mEJC amplitude.

Although we found that Amph was predominantly localized postsynaptically at the NMJ, it remains possible that low levels are present presynaptically but undetectable using immunofluorescence microscopy. These low levels could then be required for SV endocytosis and contribute to the locomotory behavior observed in both larvae and adults. If the mutations re-

sulted in chronic suppression of vesicle endocytosis, we might expect there to be a reduction in basal transmitter release. However, we found that the mutant line had maximal synaptic currents of 132.2 ± 7.2 nA ($n = 8$), while the control line had currents of 140.0 ± 8.6 nA ($n = 7$) ($p > 0.3$) in 1.0 mM Ca^{2+} , HL3 physiological solution (Figure 8A).

To determine if the *amph* mutant affected SV endocytosis in a more dynamic manner, we challenged the synapses with long trains of stimuli. First, in a moderate challenge, we delivered stimuli at 3 Hz for 10 min. This protocol led to a rapid decline in synaptic currents in *shi*¹ larval synapses, confirming this protocol induced detectable SV endocytosis (Figure 8B). In the *amph* lines we found that both the controls and the mutants maintained synaptic transmission at about 40% of their initial value for the duration of the train (1800 stimuli, Figure 8C,D), whereas responses in the *shi*¹ larvae go below 40% of their initial value after ~ 150 stimuli. When we averaged the last 10 values of the 3 Hz train, we found synaptic transmission in the *amph* control line was $39.8 \pm 0.03\%$ ($n = 5$) and in the *amph* mutant it was $44.8 \pm 0.05\%$ ($n = 5$) of

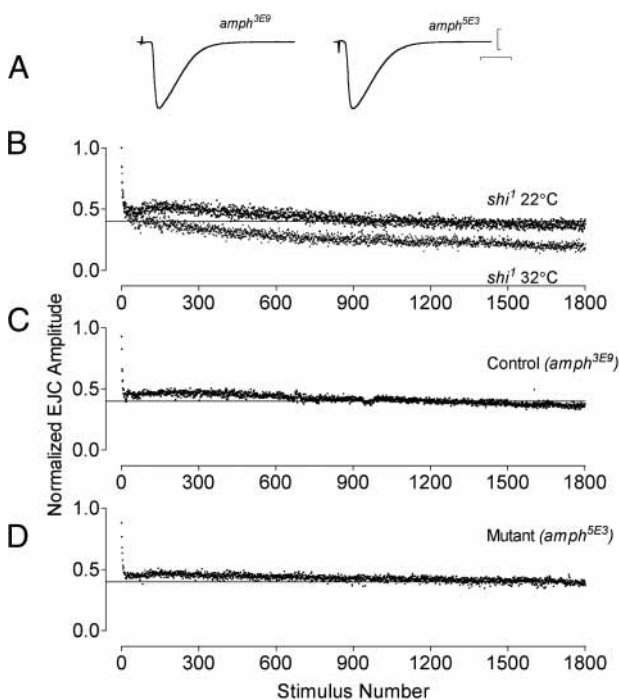


Figure 8: Synaptic fatigue in *amph* mutants. (A) Sample evoked traces from *amph*^{3E9} and *amph*^{5E3} cells. Each is the average of 20 individual traces obtained at 0.1 Hz in 1.0 mM Ca^{2+} HL3 solution. Bars: 50 nA; 10 ms (B) 3 Hz stimulation resulted in a modest but clear decline in synaptic transmission of *shi*¹ synapses at restrictive temperature (32°) compared to the permissive temperature (22°). There was no difference in the responses measured from *amph*^{5E3} (C) and *amph*^{3E9} (D) synapses. Each point represents the mean data obtained from 3 cells of *shi*¹, 5 cells from each of *amph*^{3E9} and *amph*^{5E3}. The solid line in each graph indicates the 40% level. The initial quantal content as determined from the average response to 20 stimuli delivered at 0.1 Hz.

the initial value ($p > 0.4$). Recovery from synaptic fatigue was not altered in the *amph* mutant, as we found that when stimulation frequency was reduced to 0.1 Hz, immediately following the end of the 3 Hz train, synaptic currents returned to near their initial value within ~ 4 stimuli (40 s) (data not shown) in both lines. To induce the maximal rate of vesicle endocytosis (38), we maximized transmitter release by reducing $[\text{Mg}^{2+}]$ (from 20 to 5 mM) and increasing $[\text{Ca}^{2+}]$ (from 1 to 2 mM) of the HL3 medium and delivered 2000 or 4000 stimuli at 10 Hz to the synapses. After 2000 stimuli at 10 Hz, we found EJC's in the control line were $26.0 \pm 0.01\%$ ($n = 11$) and in the *amph* mutant were $23.7 \pm 0.01\%$ ($n = 13$) of the initial quantal content. After 4000 stimuli, we found quantal content in the controls to be $19.4 \pm 0.02\%$ ($n = 6$) and in the mutants it was $17.1 \pm 0.03\%$ ($n = 6$) of the initial values. The small differences between the two genotypes are not significant ($p > 0.2$). The fractional rates of quantal secretion corresponded to ~ 1000 quanta/s and at the end of 4000 stimuli the total number of quanta secreted in the mutant was > 460000 . In a *shi* mutant background we have estimated the total vesicle pool size to be ~ 50000 quanta (B.A.S. unpublished data), in agreement with the range of results previously reported (38). This suggests that in the present experiments the total vesicle pool is turned over ~ 9 times during the course of this stimulation protocol. Taken together, we could not find evidence for either a chronic or acute impairment of SV endocytosis at the neuromuscular junction in null alleles for *Drosophila amph*.

Finally, to examine potential defects in CNS synapses that might account for the locomotory defects observed in mutants, we recorded endogenous motor output from the CNS by measuring the frequency and duration of synaptic activity from intact CNS–NMJ preparations. These experiments did not reveal a major difference in CNS-generated motor activity when *amph* mutants were compared to controls (data not shown).

Discussion

Amphiphysin was first identified as a cytosolic protein which is highly enriched in nerve terminals and partially associated with synaptic vesicles. Since then, several additional amphiphysin isoforms have been identified in mammals, yeast and nematodes, where they have been implicated in clathrin-mediated endocytosis, actin function and signaling pathways. Amphiphysin is composed of three domains which mediate its interaction with a number of endocytic proteins, such as clathrin and dynamin, suggesting that it functions as a multiprotein adaptor during clathrin-mediated endocytosis. Consistent with this model, experimental manipulations in cells using peptides or dominant-negative constructs that can block the interaction of amphiphysin with either dynamin, or clathrin and AP2, markedly inhibit clathrin-mediated endocytosis.

To further elucidate the function of amphiphysin, we characterized Amphiphysin (Amph) in *Drosophila* and generated

loss-of-function mutations. *Drosophila*, unlike vertebrates, has a single *amphiphysin* gene that gives rise to multiple isoforms by alternative splicing. Alternative splicing has also been observed in vertebrate amphiphysins, particularly amphiphysin 2 (9,39,40). In vertebrates, the largest isoform is a brain-specific 95-kDa protein that is the major amphiphysin found in the brain. In addition, several smaller isoforms have been identified, some of which are cell-type specific while others are ubiquitously expressed. This suggests that in addition to its putative role in SV endocytosis, amphiphysin 2 may have a more general role during development.

Although *Drosophila* Amph shares an equal amount of overall amino acid identity (~30%) with both Amphiphysin 1 and 2 we have identified an additional domain within *Drosophila* Amph that is conserved with Amphiphysin 2 but not Amphiphysin 1, suggesting that *Drosophila* Amph may be an Amphiphysin 2 ortholog. Consistent with this model, we also find that like Amphiphysin 2, *Drosophila* Amph is expressed throughout development and present in several tissues including muscle, CNS and imaginal discs. In most cases, we observe three predominant immuno-reactive bands on Western blots corresponding to 85kDa, 80kDa and 45kDa proteins that are not recognized with the pre-immune serum. The higher molecular weight bands likely correspond to several cDNAs that we have identified. To date, we have yet to identify any cDNAs that could correspond to the smaller 45-kDa band, and it remains possible that it represents a proteolytic product. At present, it is unclear if these represent additional splice variants or different phospho-isoforms of Amph. Several potential phosphorylation sites on *Drosophila* Amph have been identified (28) and Amphiphysin homologs are known to be phosphorylated *in vivo* (10,22,27).

To further characterize the distribution of Amph, we also performed immunohistochemical and immunofluorescence studies. Similar to what we observed using Western blot analysis, we found that Amph is broadly expressed throughout development in a variety of tissues. During early embryogenesis, Amph is found at the sites of developing membranes, epithelial cells as well as the foregut and hindgut. We did not, however, observe any Amph expression in either embryonic CNS or muscle. In contrast, Amph is expressed in both larval muscle and CNS as well as epithelial cells. Surprisingly, unlike its vertebrate counterparts, *Drosophila* Amph was predominantly found post- rather than presynaptically at the neuromuscular junction, suggesting alternative functions for the protein.

To directly assess the *in vivo* role of Amph, we characterized a series of *amph* null mutant lines that we generated by imprecise P-element mobilization. Surprisingly, all of the lines were homozygous viable although both the larvae and adults exhibited locomotory defects. This demonstrates that like yeast, Amph is not required for viability in *Drosophila*. To determine the basis of the locomotory defects in *amph* mutants, we then examined the distribution of Amph at the NMJ and determined if *amph* mutants had any defects in synaptic

morphology, physiology or synaptic vesicle endocytosis. We found no evidence for any defects in either the number of synaptic boutons or branching in our *amph* mutants.

Since Amph is localized postsynaptically at the larval neuromuscular junction, Amph may be important for regulating endocytosis of postsynaptic elements such as the glutamate receptors. If this were true, we would have predicted an effect on the amplitude of mEJCs in *amph* mutants but found no differences. Despite the abundance of Amph at postsynaptic locations, it remained possible that a low level of Amph was located within the presynaptic nerve terminal that functions in SV endocytosis. However, our physiological assessment of synaptic physiology at larval neuromuscular junctions did not reveal any chronic or acute defect in neurotransmitter release that would indicate a role for Amph in SV endocytosis at this synapse. Even under stimulation conditions which result in a nine-fold turnover of the releasable pool of SVs, we did not detect a defect in *amph* null mutants. Therefore these data suggest that Amph is not required for the normal function of the larval neuromuscular synapse.

At present, the function of Amph in *Drosophila* remains unclear. The observation that Amph is expressed postsynaptically suggests that it might act to regulate the number of neurotransmitter receptors. However, changes in receptor number would have resulted in a change in the size or distribution of the mEJCs in the *amph* mutants, which we did not observe. Nor were we able to observe any defects in the subcellular localization of two postsynaptic proteins, discs large (Dlg) and Lethal giant larvae (Lgl), which might contribute to the locomotory defects. Discs large is the *Drosophila* ortholog of PSD-95 and is thought to act as a scaffolding molecule which organizes the postsynaptic density (41). Lgl is a tumor suppressor protein which is found in epithelial cells as well as at the NMJ (29), although its function at the NMJ is unclear. We found no evidence that postsynaptic localization of either protein was affected in the *amph* mutants (P.A.L., unpublished observation). However, it remains possible that other muscle defects are responsible for the abnormal locomotion we observed in both mutant larvae and adults.

Alternatively, although Amph is not required at NMJs, it could act within CNS neurons which typically have fewer vesicles available than at NMJs and may require higher rates of SV endocytosis. Consistent with this model, we did observe Amph expression in the CNS. According to this model, Amph would not be necessary for SV endocytosis but would act to promote efficient endocytosis at specific synapses. Although surprising, our data are in fact consistent with *in vitro* binding studies which clearly demonstrate that endocytic proteins thought to be recruited by amphiphysin can assemble in the absence of amphiphysin by binding directly to each other. This suggests that amphiphysin is not required for SV endocytosis but may have evolved to promote high efficiency endocytosis.

Finally, the function of Amph may also be revealed by analyzing the role of other BAR family members. Since *Droso-*

phila Amph does not contain the conserved central domain required for interaction with other endocytic proteins, this may suggest that Amph has alternative functions within the cell. For example, the homologs of amphiphysin in budding yeast, Rvs161p and Rvs167p, not only have defects in endocytosis but also exhibit a depolarized actin cytoskeleton, as well as defects in cell polarity and bud-site selection. Although we did not detect any defects in *Drosophila amph* mutants, these may be masked by redundant proteins which act together with Amph to mediate these cellular functions. Clearly, further genetic and biochemical studies will be required to determine if Amph in *Drosophila* can interact with the actin cytoskeleton and other components of the endocytic machinery.

Materials and Methods

Fly stocks and generation of mutants

All fly stocks were maintained at room temperature on standard cornmeal agar media. Wild-type flies were Oregon-R. Mobilization of the P[EP] transposable P-element (42) insertion in *w¹¹¹⁸*; *EP(2)2175* flies (43) was used to generate both the precise excision line *amph^{3E9}*, and the imprecise excision alleles *amph^{2J6}*, *amph^{3B1}*, *amph^{5E3}*, and *amph^{6A2}*. The deficiency *amph-4A10*, which was generated at the same time as the above P-element excision, was balanced with *w^{*}*; *L² Pin¹/CyO*, *p(w⁺mC = GAL4-Kr.C)DC3*, *p(w⁺mC = UAS-GFP.S65T)DC7* (BL-5194). *Df(2R)amph-4A10* complements *l(2)k08268* (BL-P2350, Bloomington), a P-element insertion in *Sin3A*, but fails to complement both the large deficiency *vg-C* (BL-754) and *l(2)k05316* (BL-P567, Bloomington), a P-element insertion 40 kb 3' of the *EP(2)2175* insertion in the gene *spt4*. For polymerase chain reactions (PCR), genomic DNA was prepared using the single fly PCR protocol (44), with primers designed using Primer3 (S. Rozen and H.J. Skaletsky 1998, unpublished; http://www-genome.wi.mit.edu/cgi-bin/primer/primer3_www.cgi). The molecular breakpoints for all deletions were determined using a combination of Southern blot analysis and PCR with primers designed to *amph* or its two flanking genes, *Sin3A* and *Gα49B*. Additionally, all mutants complemented the lethality of the local deficiency *amph-4A10*, and *l(2)k08268*. The temperature-sensitive allele of *shibire*, *shi¹*, was obtained from Bloomington (BL-1328). The transgenic line *MHC-Gal4 UAS-CD8::Sh-GFP* (C. Goodman, University of California, Berkeley) contains the transmembrane domain of mouse CD8 fused to a small intracellular portion of the *Drosophila* Shaker K⁺ channel and to green fluorescent protein (GFP). The transgene is expressed exclusively in muscle, where it localizes to the post-synaptic membrane of the NMJ.

Amph antibody generation

The EST containing the full-length *amph* cDNA, LD19810, was subcloned into a modified pGEX-4T vector (Pharmacia) containing a C-terminal (His)₆ cassette. The sequence of the construct was verified by bi-directional sequencing. Protein expression in BSJ72 cells was induced with 1 mM IPTG, and the crude protein was purified using glutathione agarose beads (Sigma). The N-terminal GST tag was removed with thrombin protease (Sigma), and the Amph-His₆ protein was further purified with Talon cobalt resin (Clontech) and injected into rabbits for the generation of polyclonal antibodies.

Immunohistochemistry and immunoblotting

For Western blot analysis of wildtype (Oregon-R) expression, protein lysates were made from either different developmental stages (embryos, first, second and third instar larvae, early pupae, and adults) or from different tissues of third instar larvae (whole larvae, body wall, CNS, and imaginal discs). To assess Amph protein expression in *amph* mutants, lysates were

made from third instar larvae from each mutant line by homogenization of tissue in 20 μl of Ripa buffer separated by SDS-PAGE on a 10% polyacrylamide gel, transferred to a PVDF membrane, and probed with anti-Amph 9184. Equal loading was confirmed by stripping and reprobing the membrane with anti-β-tubulin antibody. Primary antibodies used were rabbit anti-Amph 9184, 1 : 1500, and mouse anti-β-tubulin, 1 : 1000. Secondary antibodies used were goat anti-rabbit IgG-HRP 1 : 10000 (Bio-Rad) and goat anti-mouse-HRP 1 : 10000 (Bio-Rad).

Immunofluorescence of wandering third instar larvae was performed as described (43). Primary antibodies used were crude or affinity-purified anti-Amph 9184, 1 : 1000 (preadsorbed with *amph^{5E3}* embryos), mouse anti-cysteine string protein (CSP), 1 : 1000 (Konrad Zinsmaier), rat anti-crumb, 1 : 500 (Ulrich Tepass), rabbit anti-gl, 1 : 200 (Fumio Matsuzaki) and rabbit anti-Dlg, 1 : 5000 (Vivian Budnik). Secondary antibodies used were goat anti-rabbit IgG-FITC, 1 : 200 (Bio-Rad), donkey anti-rabbit IgG-Cy3, 1 : 1000 and donkey anti-mouse IgG-Cy3, 1 : 1000 (Jackson Immunochemicals). Staining of the NMJs with goat anti-HRP-FITC, 1 : 500 (ICN Biomedicals, Costa Mesa, CA, USA) was performed without a secondary antibody.

Electrophysiology

Synaptic junctional currents were measured from abdominal muscle 6 of segments 3–4 using the two-electrode voltage clamp mode of an Axoclamp 2B Amplifier (Axon Instruments, Inc., Foster City, CA). For nerve stimulated experiments the nerves were cut close to the CNS and the CNS removed. For measuring endogenous motor output, the CNS and nerves were left intact. Statistical analysis was performed with Prism3 (Graphpad Software, Inc). Physiological solutions and methodology for measurements of synaptic junctional currents and data analysis are described in (45). For long trains of stimuli, we first collected baseline data by evoking 20 EJCs at a frequency of 0.1 Hz. We then increased the stimulation frequency to 3 or 10 Hz for the duration of the train. The EJC amplitudes measured during the train were normalized to the mean value of the baseline data for each cell. Quantal content was estimated for the *amph* mutant and control lines by dividing the mean EJC amplitude by the mean mEJC amplitude collected for each genotype.

Locomotion assay

Locomotion assays were performed as described in Iyengar et al. (35). One-hour embryo collections made on grape agar plates were aged 23 h and cleared of hatched larvae. After a further 1 h of aging, all hatched larvae were transferred to a 5-cm Petri dish containing fly food without cornmeal and aged to 90 h (late foraging third instar stage) at 25°C. Individual larvae were rinsed in dH₂O, and transferred to a 10-cm plate containing 1% agar to dry off for 1 min. The larva was then transferred to another 1% agar plate and allowed to habituate for 30 s before tracking was initiated. The real-time movement tracking of the larva was recorded under darkroom safelight illumination (20W incandescent lamp, Kodak GBX-2 filter) and a CCD camera (Model TSE272S, ELMO Mfg. Corp Plainview, NY) interfaced to a Scion AG-5 video rate frame grabber connected to a PowerMac 9500/200 computer. Track data were obtained using a semi-automated setup that involved a macro program written in NIH Image v1.61b (a public domain image analysis program developed at the US National Institutes of Health). The program was driven by a digitizing tablet–stylus setup (Intuos Tablet, Wacom Technology Co. WA, USA). The macro program recorded all the X–Y coordinates of the track. These data were used to create the locomotory track and to calculate the distance traveled by the larva in 30 s. The data were analyzed with Prism 3 (Graphpad Software, Inc.).

Acknowledgments

We thank C. Goodman for providing the CD8:Sh-GFP flies and C.C. Hui for the GST-His₆ vector. We also thank the following individuals for kindly

providing us with antibodies to the following proteins: K. Zinsmaier (CSP), U. Tepass (crb); F. Matsuzaki (1(2)gl) and V. Budnik (dlg). We also thank U. Tepass and W.S. Trimble for useful discussions and W.S. Trimble for critical comments on the manuscript. Finally, we also wish to thank C. Doe for sharing information prior to publication. This work was supported by funds from the Canadian Institutes of Health Research to G.L.B. and Doctoral Research Awards to P.A.L. and B.M.C. G.L.B. is the recipient of a CIHR Investigator award and B.A.S. is the recipient of a Post-doctoral Fellowship from the Hospital for Sick Children Research Training Center.

References

- De Camilli P, Takei K. Molecular mechanisms in synaptic vesicle endocytosis and recycling. *Neuron* 1996;16:481–486.
- De Camilli P, Takei K, McPherson PS. The function of dynamin in endocytosis. *Curr Opin Neurobiol* 1995;5:559–565.
- Stowell MHB, Marks B, Wigge P, McMahon HT. Nucleotide-dependent conformational changes in dynamin: evidence for a mechanochemical molecular spring. *Nat Cell Biol* 1999;1:27–32.
- Sever S, Muhlberg AB, Schmid SL. Impairment of dynamin's GAP domain stimulates receptor-mediated endocytosis. *Nature* 1999;398:481–486.
- McPherson PS, Garcia EP, Slepnev VI, David C, Zhang X, Grabs D, Sossin WS, Bauerfeind R, Nemoto Y, De Camilli P. A presynaptic inositol-5-phosphatase. *Nature* 1996;379:353–357.
- Schmidt A, Wolde M, Thiele C, Fest W, Kratzin H, Podtelejnikov AV, Witke W, Huttner WB, Soling HD. Endophilin I mediates synaptic vesicle formation by transfer of arachidonate to lysophosphatidic acid. *Nature* 1999;401:133–141.
- Lichte B, Veh RW, Meyer HE, Kilimann MW. Amphiphysin, a novel protein associated with synaptic vesicles. *EMBO J* 1992;11:2521–2530.
- Ramjaun AR, Micheva KD, Bouchelet I, McPherson PS. Identification and characterization of a nerve terminal-enriched amphiphysin isoform. *J Biol Chem* 1997;272:16700–16706.
- Sakamuro D, Elliott KJ, Wechsler-Reya R, Prendergast GC. BIN1 is a novel Myc-interacting protein with features of a tumour suppressor. *Nat Genet* 1996;14:69–77.
- Wigge P, Vallis Y, McMahon HT. Inhibition of receptor-mediated endocytosis by the amphiphysin SH3 domain. *Curr Biol* 1997;7:554–560.
- Ramjaun AR, Philie J, de Heuvel E, McPherson PS. The N terminus of amphiphysin II mediates dimerization and plasma membrane targeting. *J Biol Chem* 1999;274:19785–19791.
- McMahon HT, Wigge P, Smith C. Clathrin interacts specifically with amphiphysin and is displaced by dynamin. *FEBS Lett* 1997;413:319–322.
- Slepnev VI, Ochoa G-C, Butler MH, Grabs D, De Camilli P. Role of phosphorylation in regulation of the assembly of endocytic coat complexes. *Science* 1998;281:821–824.
- Ramjaun AR, McPherson PS. Multiple amphiphysin II splice variants display differential clathrin binding: identification of two distinct clathrin-binding sites. *J Neurochem* 1998;70:2369–2376.
- Leprince P, Romero F, Cussac D, Vayssiere B, Berger R, Tavitian A, Camonis JH. A new member of the amphiphysin family connecting endocytosis and signal transduction pathways. *J Biol Chem* 1997;272:15101–15105.
- David C, McPherson PS, Mundigl O, De Camilli P. A role of amphiphysin in synaptic vesicle endocytosis suggested by its binding to dynamin in nerve terminals. *Proc Natl Acad Sci USA* 1996;93:331–335.
- Shupliakov O, Low P, Grabs D, Gad H, Chen H, David C, Takei K, De Camilli P, Brodin L. Synaptic vesicle endocytosis impaired by disruption of dynamin-SH3 domain interactions. *Science* 1997;276:259–263.
- Volchuk A, Narine S, Foster LJ, Grabs D, De Camilli P, Klip A. Perturbation of dynamin II with an amphiphysin SH3 domain increases GLUT4 glucose transporters at the plasma membrane in 3T3-L1 adipocytes. Dynamin II participates in GLUT4 endocytosis. *J Biol Chem* 1998;273:8169–8176.
- Cestra G, Castagnoli L, Dente L, Minenkova O, Petrilli A, Mignone N, Hoffmuller U, Schneider-Mergener J, Cesareni G. The SH3 domains of endophilin and amphiphysin bind to the proline-rich region of synaptotagmin 1 at distinct sites that display an unconventional binding specificity. *J Biol Chem* 1999;274:32001–32007.
- Slepnev VI, Ochoa GC, Butler MH, De Camilli P. Tandem arrangement of the clathrin and AP-2 binding domains in amphiphysin 1 and disruption of clathrin coat function by amphiphysin fragments comprising these sites. *J Biol Chem* 2000;275:17583–17589.
- Munn AL, Stevenson BJ, Geli MI, Reizman H. end5, end6 and end7: mutations that cause actin delocalization and block the internalization step of endocytosis in *Saccharomyces cerevisiae*. *Mol Biol Cell* 1995;6:1721–1742.
- Lee J, Colwill K, Anelunas V, Tennyson C, Moore L, Ho Y, Andrews B. Interaction of yeast Rvs167 and Pho85 cyclin-dependent kinase complexes may link the cell cycle to the actin cytoskeleton. *Curr Biol* 1998;8:1310–1321.
- Crouzet M, Urdaci M, Dulau L, Aigle M. Yeast mutant affected for viability upon nutrient starvation. characterization and cloning of the RVS161 gene. *Yeast* 1991;7:727–743.
- Bauer F, Urdaci M, Aigle M, Crouzet M. Alteration of a yeast SH3 protein leads to conditional viability with defects in cytoskeletal and budding patterns. *Mol Cell Biol* 1993;13:5070–5084.
- Sivadon P, Bauer F, Aigle M, Crouzet M. Actin cytoskeleton and budding pattern are altered in the yeast rvs161 mutant: the RVS161 protein shares common domains with the brain protein amphiphysin. *Mol Gen Genet* 1995;246:484–495.
- Balguerie A, Sivadon P, Bonneau M, Aigle M. Rvs167p, the budding yeast homolog of amphiphysin, colocalizes with actin patches. *J Cell Sci* 1999;112:2529–2537.
- Floyd SR, Porro EB, Slepnev VI, Ochoa GC, Tsai LH, De Camilli P. Amphiphysin binds the cdk5 regulatory subunit p35 and is phosphorylated by cdk5 and cdc2. *J Biol Chem* 2001;276:8104–8110.
- Razzaq A, Su Y, Mehren JE, Mizuguchi K, Jackson AP, Gay NJ, O'Kane CJ. Characterization of the gene for *Drosophila* amphiphysin. *Gene* 2000;41:167–174.
- Lloyd TE, Verstreken P, Ostrin EJ, Phillippi A, Lichtarge O, Bellen HJ. A genome-wide search for synaptic vesicle cycle proteins in *Drosophila*. *Neuron* 2000;26:25–50.
- Neufeld TP, Tang AH, Rubin GM. A genetic screen to identify components of the sina signaling pathway in *Drosophila* eye development. *Genetics* 1998;148:277–286.
- Penneta G, Pauli D. The *Drosophila* Sin3 gene encodes a widely distributed transcription factor essential for embryonic viability. *Dev Genes Evol* 1998;208:531–536.
- Lee YJ, Dobbs MB, Verardi ML, Hyde DR. dgq: a *Drosophila* gene encoding a visual system-specific G alpha molecule. *Neuron* 1990;5:889–898.
- Strathmann M, Simon MI. G protein diversity: a distinct class of alpha subunits is present in vertebrates and invertebrates. *Proc Natl Acad Sci USA* 1990;87:9113–9117.
- Marsh M, McMahon HT. The structural era of endocytosis. *Science* 1999;285:215–220.
- Iyengar B, Roote J, Campos AR. The tams gene, identified as a mutation that disrupts larval behavior in *Drosophila melanogaster*, codes for the mitochondrial DNA polymerase catalytic subunit (DNApol-gamma125). *Genetics* 1999;153:1809–1824.
- January LY, January YN. Properties of the larval neuromuscular junction in *Drosophila melanogaster*. *J Physiol (London)* 1976;262:189–214.

Leventis et al.

37. Sokal RR, Rohlf FJ. Biometry. San Francisco: W.H. Freeman; 1969.
38. Delgado R, Maureira C, Oliva C, Kidokoro Y, Labarca P. Size of vesicle pools, rates of mobilization, and recycling at neuromuscular synapses of a *Drosophila* mutant, shibire. *Neuron* 2000;28:941–953.
39. Butler MH, Ochoa DC, Freyberg Z, Daniell L, Grabs D, Cremona O, De Camilli P. Amphiphysin II (SH3P9;BIN1), a member of the amphiphysin/Rvs family, is concentrated in the cortical cytomatrix of axon initial segments and nodes of ranvier in brain and around T tubules in skeletal muscle. *J Cell Biol* 1997;137:1355–1367.
40. Wechsler-Reya R, Sakamura D, Zhang J, Duhadaway J, Prendergast GC. Structural analysis of the BIN1 gene. Evidence for tissue-specific transcriptional regulation and alternate RNA splicing. *J Biol Chem* 1997;272:31453–31458.
41. Lahey T, Gorczyca M, Jia XX, Budnik V. The *Drosophila* tumor suppressor gene *dlg* is required for normal synaptic bouton structure. *Neuron* 1994;13:823–835.
42. Rorth P. A modular misexpression screen in *Drosophila* detecting tissue-specific phenotypes. *Proc Natl Acad Sci USA* 1996;93:12418–12422.
43. Rorth P, Szabo K, Bailey A, Laverty T, Rehm J, Rubin GM, Weigmann K, Milan M, Benes V, Ansorge W, Cohen SM. Systemic gain-of-function genetics in *Drosophila*. *Development* 1998;125:1049–1057.
44. Gloor GB, Preston CR, Johnson-Schlitz DM, Nassif NA, Phillis RW, Benz WK, Robertson HM, Engels WR. Type I repressors of P element mobility. *Genetics* 1993;135:81–95.
45. Stewart BA, Mohtashami M, Trimble WS, Boulianne GL. SNARE Proteins contribute to calcium cooperativity of synaptic transmission. *Proc Natl Acad Sci USA* 2000;97:13955–13960.
46. Frerking M, Borges S, Wilson M. Variation in GABA mini amplitude is the consequence of variation in transmitter concentration.. *Neuron* 1995;15:885–895.